Generation of a Sheared Plasma Rotation by Emission, Propagation, and Absorption of Drift Wave Packets

M. Xu,[1,3] G. R. Tynan,[1,3] P. H. Diamond,[1,2,4] C. Holland,[3] J. H. Yu,[3] and Z. Yan[5]

[1]*Center for Momentum Transport and Flow Organization, University of California at San Diego, San Diego, California, USA*
[2]*Center for Astrophysics and Space Science and Department of Physics, University of California at San Diego, San Diego, California, USA*
[3]*Center for Energy Research and Department of Mechanical and Aerospace Engineering, University of California at San Diego, San Diego, California, USA*
[4]*WCI Center for Fusion Theory, National Fusion Research Institute, Gwahangno 113, Yusung-gu, Daejeon 305-333, Korea*
[5]*Department of Engineering Physics, University of Wisconsin–Madison, Madison, Wisconsin 53706, USA*

(Received 21 June 2010; published 28 July 2011)

Collisional electron drift wave turbulence generates drift wave packet structures with density and vorticity fluctuations in the central plasma pressure gradient region of a linear plasma device. Tracking these packets reveals that they follow an outward directed spiral-shaped trajectory in the (r, θ) plane, are azimuthally stretched, and develop anisotropy as they approach an axisymmetric, radially sheared azimuthal flow located at the plasma boundary. Nonlinear energy transfer measurements and time-delay analysis confirm that structure absorption amplifies the sheared flow. Similar mechanisms likely operate at the edge of confined toroidal plasmas and should lead to the amplification of sheared flows at the boundary of these devices as well.

DOI: 10.1103/PhysRevLett.107.055003 PACS numbers: 52.35.Ra, 52.35.Mw

The generation of intrinsic rotation in toroidally confined plasmas, in which the plasma spontaneously rotates in the toroidal direction without direct toroidal momentum input, has been attributed to the existence of a nondiffusive residual turbulent stress localized to the plasma boundary [1]. Measurements in tokamak experiments [2,3] and a linear plasma device [4] provide evidence that residual stress does indeed exist at the plasma boundary. However, this earlier work did not identify the operative *microscopic* physics mechanism that leads to the generation of such a stress at the plasma boundary. In this Letter, we show how this residual stress is caused by the emission of isotropic turbulent drift vortices from the inner plasma region which spiral outward. As these structures approach the shear layer at the plasma boundary, they are stretched azimuthally, become increasingly anisotropic, and then are absorbed into the shear layer, thereby transferring their momentum and energy to the shear layer, which is consequently amplified. This mechanism is likely to be operative in toroidal confinement devices and also is similar to mechanisms operating in other fluid systems [5] and therefore should be of broad interest.

These experiments were carried out in the Controlled Shear Decorrelation Experiment, which is a 2.8 m long linear helicon plasma device with a source radius $r_{\mathrm{src}} = 4.5$ cm, 1.5 kW rf power input (reflected power less than 30 W), and a gas fill pressure of 3.2 mTorr. The exit plane of the source defines the axial position $z = 0$ cm. Details of the apparatus plasma conditions and earlier physics results can be found in the literature [6–14].

Heat input from the rf source sustains a centrally peaked plasma density [Fig. 1(a)] and electron temperature profile [7] (not shown here), thus driving an electron pressure gradient in the region $r < 5$ cm, with a peak density gradient located at $r = 3$ cm [Fig. 1(b)]. A time-averaged azimuthally symmetric sheared azimuthal flow $\langle v_\theta \rangle$ exists [Fig. 1(c)] and has a negative vorticity $\omega_{\mathrm{ZF}} = \nabla_r \langle v_\theta \rangle = \langle V_E' \rangle < 0$ in the shear layer at $r = 3.5$–4 cm. The plasma column maintains this intrinsic rotation by the combined action of turbulent stresses and a no-slip boundary condition due to ion-neutral drag [4]. We also note that the peak density gradient occurs slightly inside the shear layer.

The sheared flow grows over a few millisecond period [12] and then undergoes a more rapid (hundreds of microseconds) collapse when a plasma blob is ejected into the region $r > 5$ cm [15]. During the shear flow growth phase, the turbulence is characterized by fluctuations with azimuthal wave number $k_\theta \geq 1\ \mathrm{cm}^{-1}$, corresponding to an effective azimuthal mode number $m_{\mathrm{eff}} \equiv k_\theta r \geq 3$ for $r = 3$ cm with a frequency $f \geq 6$ kHz [12], while during the collapse phase the central plasma fluctuations are dominated by a global $m = 1$ oscillation with $f \sim 2$–4 kHz. Since in this Letter we are focused on the generation mechanism of the shear flow, we apply a nonrecursive finite impulse response high-pass digital filter using a Kaiser window to the imaging and probe fluctuation data. This gives an amplitude suppression ratio >5 within 1 kHz of the 5 kHz cutoff frequency and a ratio as high as 10^6 with sufficient frequency width [16] and thereby isolates the growth phase of the sheared flow which we focus on here.

A 28 cm diameter $f/10$ telescope coupled to a digital fast-framing (100 000 frames/sec) camera located ~8 m

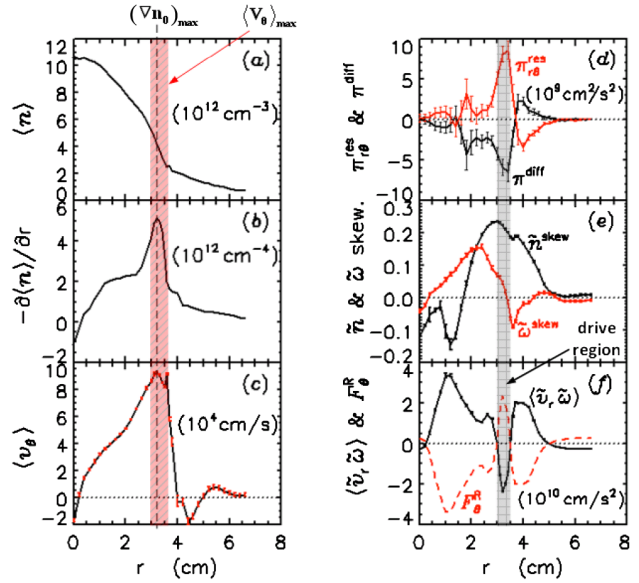

FIG. 1 (color online). Time-averaged radial profiles of the Controlled Shear Decorrelation Experiment plasma. (a) Time-averaged density n_0. (b) Gradient of the time-averaged density $-\partial n_0/\partial r$. (c) Time-averaged azimuthal velocity $\langle V_\theta \rangle$. (d) Residual stress $\pi^{\rm res}_{r\theta}$ (solid red line) and the diffusive momentum flux $\pi^{\rm diff} \equiv -\langle \tilde{v}_r^2 \rangle \tau_c \frac{\partial \langle V_\theta \rangle}{\partial r}$ (solid black line). (e) Skewness of density (solid black line) and vorticity (solid red line) fluctuations. (f) Time-averaged radial flux of vorticity $\langle \tilde{v}_r \tilde{\omega} \rangle$ (solid black line) and Reynolds force F^R_θ due to turbulent vorticity (dashed red line).

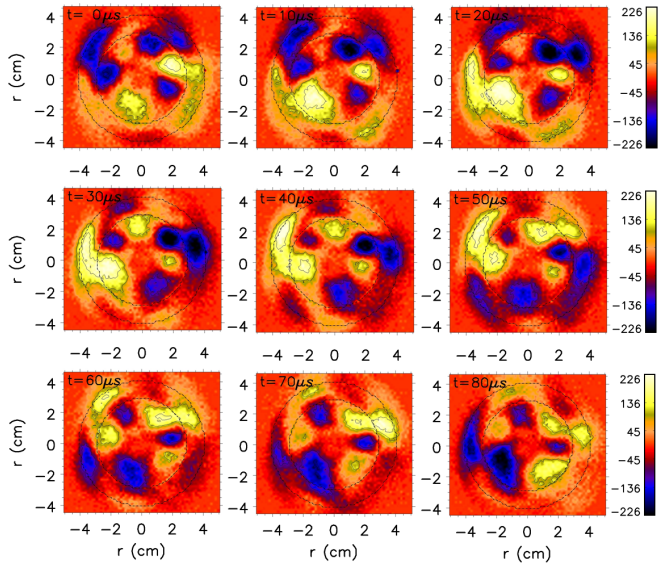

FIG. 2 (color online). Sequential visible light emissions images showing the birth, evolution, and death of vortexlike structures. Radii of $r = 3.0$ cm and $r = 4.0$ cm are denoted by the two dashed circles.

away from the object focal plane located at $z = 75$ cm provides a view with sight lines aligned within $\pm 0.7°$ of the magnetic field lines. The camera detects visible light intensity fluctuations $\tilde{I}_{\rm vis}$ (due primarily to neutral argon emission) as shown in Fig. 2. These $\tilde{I}_{\rm vis}$ fluctuations are correlated with $I_{\rm sat}$ Langmuir probe fluctuations [17]. The initially isotropic $m \sim 3$ structures with frequency $f \geq 6$ kHz are born between the plasma center and the maximum density gradient at $r \sim 3$ cm and propagate primarily in the electron diamagnetic drift direction. We directly measured the nonlinear kinetic energy transfer term $T_u(f) = -{\rm Re} \sum_{f_1} \tilde{u}_f \cdot (\tilde{u}_{f-f_1} \cdot \nabla \tilde{u}_{f_1})$ [13] at $z = 75$ cm and $r \sim 2$ cm and then mapped the results into the k_θ domain [14]. The result $T_u(k_\theta)$ is shown in Fig. 3(a) (dotted blue line) and indicates that the $m \sim 3$ structures born at $r = 2$–3 cm are generated by the nonlinear transfer of kinetic energy from other spatial scales with $m > 0$ into the $m = 3$ structures and are thus nonlinearly pumped drift turbulence structures or wave packets.

Since these structures have correlated density $\tilde{n}$ and potential $\tilde{\phi}$ fluctuations [7], and since the resulting vorticity fluctuations $\tilde{\omega} \equiv \nabla \times \tilde{v}_E$ (where $\tilde{v}_E \equiv \frac{\vec{B} \times \nabla \tilde{\phi}}{B^2}$ is the fluctuating electrostatic $E \times B$ velocity) are given by $\tilde{\omega} \equiv \frac{1}{B} \nabla^2 \tilde{\phi}$, the vorticity fluctuations should be correlated with density fluctuations as expected from the Hasagawa-Wakatani model of collisional drift turbulence where in the limit of vanishing cross-field collisional diffusion total potential vorticity $q \equiv \ln n_0 + \frac{\tilde{n}}{n_0} - \frac{e \rho_s^2}{k T_e} \nabla^2 \tilde{\phi} = {\rm const}$ is an inviscid invariant along fluid trajectories. Here, n_0 varies slowly in time as compared to fluctuating quantities; therefore, $q \approx \tilde{q} = {\rm const}$. Simultaneous measurements of $\tilde{I}_{\rm sat}$ and $\tilde{\omega}$ with the 3×3 probe array [13] show that this is indeed the case [Figs. 3(b) and 3(c)] and that the vorticity has roughly a zero time delay with respect to the density fluctuations, suggesting that indeed $\tilde{q}$ is conserved in this region. Fast imaging thus also reveals the birth, evolution, motion, and death of vorticity fluctuations.

Examining Fig. 2 carefully, we also observe that the structure motion contains an outward radial component in addition to the azimuthal component, and thus the structures gradually move outwards in a spiral-shaped trajectory. As the structures approach the shear layer located at $r = 3.5$ cm (which is within the region between the two circles shown in each panel of Fig. 2), their radial propagation slows as they undergo a "tilt-stretch-absorption" (TSA) process. In the course of this, their radial correlation length is reduced [10]. They tilt and become increasingly anisotropic and ultimately are absorbed by the shear layer. This TSA behavior is reminiscent of the Howard-Krishnamurti process [5] by which a series of two-dimensional convective rolls tilt, stretch, and then merge to form a larger scale eddy; the difference here is that a smaller scale eddy or structure is interacting with a preexisting larger scale $m = 0$ sheared flow. Eddies also occasionally break up into several smaller scaled eddies.

Probe measurements show that the $I_{\rm sat}$ skewness [Fig. 1(e), solid black line] changes sign near $r = 2$ cm, suggesting that the turbulent radial velocity fluctuations give rise to outward (inward) going positive (negative) density perturbations which modulate the density gradient

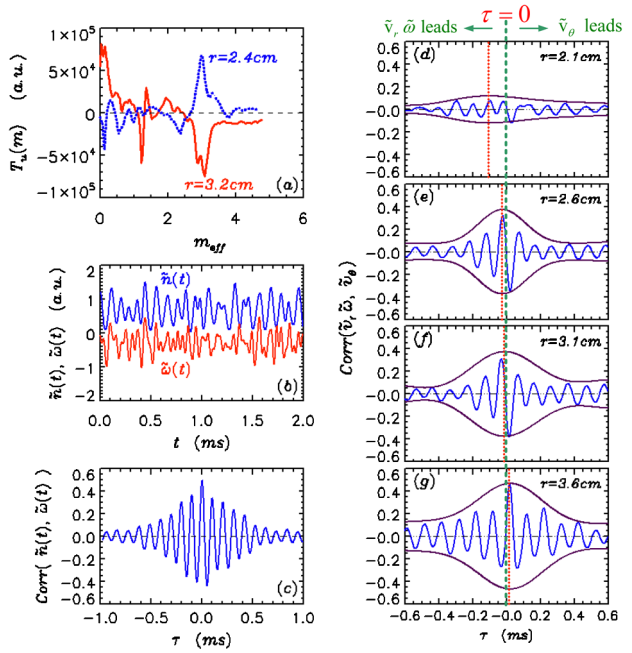

FIG. 3 (color online). (a) Nonlinear kinetic energy transfer vs effective azimuthal mode number at $r = 2.4$ cm (dashed black line) corresponding to the vortex structures generation region and $r = 3.2$ cm (solid red line) corresponding to the location of the shear layer. A positive (negative) T_u value indicates a gain (loss) of turbulent kinetic energy through nonlinear processes. The statistical noise level was estimated as $\sim 1/\sqrt{N} < 3\%$ (N is the number of realizations) and thus is negligibly small. (b) Time-resolved density (blue) and vorticity (red) fluctuations. (c) Correlation between density and vorticity fluctuations, which shows that density and vorticity fluctuations have a significant correlation with zero phase shift. (d)–(g) Cross correlation between vorticity flux at different radial positions [(d)–(g) correspond to $r = 2.1$, 2.6, 3.1, and 3.6 cm, respectively] and turbulent azimuthal velocity in the shear layer at $r = 3.6$ cm. An increase in central plasma vorticity flux leads to a subsequent increase in the boundary plasma azimuthal velocity ~ 110 μs later. Solid blue lines are the calculated correlations. Up-down symmetric envelopes (solid purple line) were computed from the correlations; the center of each envelope is indicated by the dotted red vertical lines. The dotted green line corresponds to zero time delay.

in this region and drive outward particle transport, consistent with previous turbulent particle flux measurements [7]. The vorticity fluctuation skewness is positive in the region between $0 < r < 3.0$ cm and is peaked near $r = 2$ cm [Fig. 1(e), solid red line], indicating that an excess of positive vorticity events occur in the region where the positive density events are born. Correlated measurements of $\tilde{v}_r(t) = -\frac{\nabla_\theta \tilde{\phi}_f(t)}{B}$ and $\tilde{\omega}(t)$ from the 3×3 probe array show a positive flux of vorticity, $\langle \tilde{v}_r \tilde{\omega} \rangle$ [Fig. 1(f), solid black line]. However, examining Figs. 1(e) and 1(f) in detail, we find that the vorticity skewness and vorticity flux change sign and become negative in the region $3.0 < r < 3.5$ cm. The imaging results (Fig. 2) show that the structures, which have vorticity associated with them, are still moving outwards (albeit at a slower rate) and therefore have on average $\tilde{v}_r > 0$ in this region. We can therefore infer that, on average, the sign of the vorticity of the structures is changed in this region.

Noting that the $m = 0$ flow shearing rate $\nabla_r \langle v_\theta \rangle = \omega_{\rm ZF} \approx \omega_{\rm sh} \approx -8 \times 10^4$ sec$^{-1} < 0$ as discussed above and estimating that $\tilde{\omega} \approx \tau_{\rm eddy}^{-1} \approx \frac{\tilde{\phi}}{BL_\perp^2} \approx 1 - 6 \times 10^4$ sec^{-1} for the observed rms floating potential fluctuation amplitude $\tilde{\phi}_f \approx 0.3$–$0.6$ V and perpendicular structure scale length $L_\perp \approx 1$–2 cm, we find that $|\omega_{\rm ZF}| > |\tilde{\omega}|$. Here $\tau_{\rm eddy}^{-1}$ is the eddy rotation rate, and $\omega_{\rm sh}$ is the flow shearing rate. Hence a crude estimate based on the Okubo-McWillaims-Weiss criteria [18] for evolution of the local vorticity gradient, namely, $\partial_t \nabla \omega \propto (V'^2 - \omega^2)^{1/2}$, suggests that $\partial_t \nabla \omega > 0$ near the shear layer, where $V' > \omega \sim \frac{1}{\tau_{\rm eddy}}$ as noted above. This steepening of the vorticity gradient drives a forward enstrophy transfer to small scales, which effectively then peels apart the eddy. Thus when the weaker (i.e., $|\omega_{\rm ZF}| > |\tilde{\omega}|$) small-scale positive vorticity structure encounters the large-scale shear layer with strong negative vorticity, a progressive merging process occurs during which the outer layers of the smaller structure are sequentially peeled off , leading to the eventual absorption of the smaller structure by the stronger large-scale shear flow. This picture is consistent with the vorticity flux profile [Fig. 1(f)] and with recently published results from neutral fluids and plasmas [19–21]. Small structures with negative vorticity, which are rarer in the central plasma region [Fig. 1(e)], will be readily absorbed by the negative vorticity mean shear layer. The net contribution from small structures with positive vorticity and those with negative vorticity results in a transfer of the structure's turbulent kinetic energy into the shear layer as shown by measurements of $T_u(k_\theta)$ at $r = 3.0$–4.0 cm [Fig. 3(a), solid red curve].

For these $E \times B$-dominated turbulent flows which have azimuthally invariant fluctuation statistics, the Taylor identity [22] holds and shows that the vorticity flux is related to the turbulent Reynolds stress and Reynolds force F_θ^R exerted by the fluctuations upon the background plasma by the relation $F_\theta^R = -\nabla_r \langle \tilde{v}_r \tilde{v}_\theta \rangle = -\langle \tilde{v}_r \tilde{\omega} \rangle$ [22,23]. Our previous work shows that, for the estimated dissipation profiles, F_θ^R is consistent with the mean shear flow and that the slow variations in F_θ^R are also consistent with slow changes in the shear flow [12]. Examining Fig. 1(f), we find that $\langle \tilde{v}_r \tilde{\omega} \rangle < 0$ for $3 < r < 3.5$ cm and has values consistent with the previously published total Reynolds stress profile (quantitatively, in the shear region the peak amplitude of $\langle \tilde{v}_r \tilde{\omega} \rangle$ is about 30% less than $\nabla_r \langle \tilde{v}_r \tilde{v}_\theta \rangle$ inferred from the measured Reynolds stress profile). The Reynolds force F_θ^R resulting from the vorticity flux thus amplifies the shear flow in the plasma boundary region. A cross-correlation analysis between the instantaneous fluctuating vorticity flux at variable positions $r < 3.6$ cm and the instantaneous turbulent azimuthal velocity at the shear

layer at $r = 3.6$ cm shows that an increase in vorticity flux from the central plasma region *precedes* an increase in the turbulent azimuthal velocity at the shear layer maximum [Figs. 3(d)–3(g)]. Similarly, the cross correlation between turbulent vorticity flux at variable positions $r < 3.6$ cm and turbulent Reynolds stress at the shear layer was evaluated and showed a similar causal relationship. Both correlations, then, confirm that vortices mediate the spatial transport of turbulent momentum from the central plasma region into the shear layer.

The TSA mechanism may also be understood as a consequence of shear-induced refraction and its impact on wave packet energetics. Since wave packet action density (closely linked to potential enstrophy density) is conserved in a spatiotemporally adiabatic shearing field [24], the wave packet energy density then evolves according to $\frac{d\varepsilon}{dt} = \frac{\partial\omega_k}{\partial k_r}\frac{dk_r}{dt}\frac{\varepsilon}{\omega_k} = -k_\theta v_{gr}\langle V_E'\rangle\varepsilon/\omega_k$, where wave packets obey a dispersion relation ω_k. Since $v_{gr} = -\frac{2k_r k_\theta \rho_S^2}{1+k_\perp^2\rho_S^2} v_*$ and by taking $k_r = k_r^{(0)} - k_\theta\langle V_E'\rangle\tau$, this means that $\frac{d\varepsilon}{dt} = \frac{-2k_\theta^2\rho_S^2}{(1+k_\perp^2\rho_S^2)}\langle V_E'\rangle^2\tau_L\varepsilon$, where V_E' denotes the shear strength, τ_L denotes the lifetime of the wave packet, and we took $|k_\theta\langle V_E'\rangle\tau| > k_r^{(0)}$ for simplicity. Note that wave packet energy decreases due to shearing, at a rate that is quadratic in the shear strength. As shown elsewhere [24], the total energy is conserved in the course of the straining interaction, so that $\frac{d}{dt}(\varepsilon + \langle V_E\rangle^2) = 0$ for a suitably normalized shear flow velocity, meaning that flow energy $\langle V_E\rangle^2$ increases at the expense of the wave packet energy. This simple calculation, then, quantifies the intuitive concept of the TSA mechanism, whereby shear flows strain and stretch wave packets and so ultimately consume their energy. The TSA mechanism may also be viewed as a type of strongly anisotropic inverse cascade, though we emphasize that it is not intrinsically statistical. These results also imply that wave stresses naturally act to amplify sheared flows. This follows simply from the fact that for electrostatic $E \times B$ flows $\langle\tilde{v}_r\tilde{v}_\theta\rangle = \frac{1}{B_0^2}\langle k_r k_\theta|\tilde{\phi}_k|^2\rangle$ and so for $k_r = k_r^{(0)} - k_\theta\langle V_E'\rangle\tau$, the shearing breaks symmetry so as to render $\langle k_r k_\theta\rangle$ unambiguous. Thus $\langle\tilde{v}_r\tilde{v}_\theta\rangle \approx -k_\theta^2\rho_S^2\langle\frac{e\tilde{\phi}}{k_B T_e}\rangle^2 C_S^2\langle V_E'\rangle\tau$, and comparison with the discussion above then shows that $\frac{d\varepsilon}{dt} = \langle\tilde{v}_r\tilde{v}_\theta\rangle\langle V_E'\rangle$, which is clearly equivalent to the Reynolds work performed by the wave stress on the mean shear flow.

Finally, we observe that, in toroidal geometry, the TSA realization of the perpendicular stress, $\langle\tilde{v}_r\tilde{v}_\perp\rangle$, will have a finite toroidal projection and so may drive intrinsic toroidal rotation. Furthermore, we note that the plasma edge of tokamaks and linear devices has been shown to generate plasma density "blobs" and "holes" [25–27]; the blobs propagate outwards, while the holes propagate inwards and have vorticity associated with them [26,28]; this region of toroidally confined plasmas has long been known to have a shear layer present due to equilibrium effects at the last closed flux surface. Thus a radial vorticity flux and associated wave stresses must exist at the boundary of the tokamak plasmas in precisely the region where the *L-H* transition and intrinsic rotation appear to originate; this flux and wave stress may then contribute to shear flow amplification and intrinsic rotation in these devices. Similar experiments should be repeated on large tokamaks to confirm the above physical picture, particularly where there will be a clearer scale separation between turbulent correlation lengths and the scale length from generation to damping locations. These results also show that particle flux and vorticity flux are closely related and suggest that potential vorticity conservation plays an important role in momentum transport in confined plasmas, much like in planetary and stellar atmospheres [29]. These issues are now under investigation and will be discussed in future publications [30].

[1] P. H. Diamond *et al.*, Nucl. Fusion **49**, 045002 (2009).
[2] J. E. Rice *et al.*, Nucl. Fusion **44**, 379 (2004).
[3] W. M. Solomon *et al.*, Plasma Phys. Controlled Fusion **49**, B313 (2007).
[4] Z. Yan *et al.*, Phys. Rev. Lett. **104**, 065002 (2010).
[5] L. N. Howard and R. Krishnamurti, J. Fluid Mech. **170**, 385 (1986).
[6] G. R. Tynan *et al.*, J. Vac. Sci. Technol. A **15**, 2885 (1997).
[7] M. J. Burin *et al.*, Phys. Plasmas **12**, 052320 (2005).
[8] C. Holland *et al.*, Phys. Rev. Lett. **96**, 195002 (2006).
[9] G. R. Tynan *et al.*, Plasma Phys. Controlled Fusion **48**, S51 (2006).
[10] Z. Yan *et al.*, Phys. Plasmas **15**, 092309 (2008).
[11] Z. Yan *et al.*, Phys. Plasmas **17**, 012302 (2010).
[12] Z. Yan *et al.*, Phys. Plasmas **17**, 032302 (2010).
[13] M. Xu *et al.*, Phys. Plasmas **16**, 042312 (2009).
[14] M. Xu *et al.*, Phys. Plasmas **17**, 032311 (2010).
[15] S. H. Müller *et al.*, Plasma Phys. Controlled Fusion **51**, 055020 (2009).
[16] A. V. Oppenheim, R. W. Schafer, and J. R. Buck, *Discrete-Time Signal Processing*, (Prentice-Hall, Upper Saddle River, NJ, 1999), Chap. 7, p. 474, 2nd ed.
[17] G. Y. Antar *et al.*, Phys. Plasmas **14**, 022301 (2007).
[18] J. C. McWilliams, J. Fluid Mech. **146**, 21 (1984).
[19] R. R. Trieling *et al.*, Phys. Fluids **17**, 087103 (2005).
[20] P. Manz, M. Ramisch, and U. Stroth, Phys. Rev. Lett. **103**, 165004 (2009).
[21] P. Manz *et al.*, Plasma Phys. Controlled Fusion **51**, 035008 (2009).
[22] G. I. Taylor, Phil. Trans. R. Soc. A **215**, 1 (1915).
[23] P. H. Diamond *et al.*, Plasma Phys. Controlled Fusion **50**, 124018 (2008).
[24] P. H. Diamond *et al.*, Plasma Phys. Controlled Fusion **47**, R35 (2005).
[25] S. I. Krasheninnikov, Phys. Lett. A **283**, 368 (2001).
[26] J. A. Boedo *et al.*, Phys. Plasmas **10**, 1670 (2003).
[27] G. S. Xu *et al.*, Nucl. Fusion **49**, 092002 (2009).
[28] O. Grulke *et al.*, Phys. Plasmas **13**, 012306 (2006).
[29] D. G. Dritschel and M. E. McIntyre, J. Atmos. Sci. **65**, 855 (2008).
[30] C. J. McDevitt *et al.*, Phys. Plasmas **17**, 112509 (2010).